

Article

Creep of Polycrystalline Magnesium Aluminate Spinel Studied by an SPS Apparatus

Barak Ratzker, Maxim Sokol, Sergey Kalabukhov and Nachum Frage *

Department of Materials Engineering, Ben-Gurion University of the Negev, P.O. Box 653, Beer-Sheva 84105, Israel; ratzkerb@post.bgu.ac.il (B.R.); sokolmax@bgu.ac.il (M.S.); kalabukh@bgu.ac.il (S.K.)

* Correspondence: nfrage@bgu.ac.il; Tel.: +972-8-646-1468

Academic Editor: Eugene A. Olevsky

Received: 8 May 2016; Accepted: 16 June 2016; Published: 20 June 2016

Abstract: A spark plasma sintering (SPS) apparatus was used for the first time as an analytical testing tool for studying creep in ceramics at elevated temperatures. Compression creep experiments on a fine-grained (250 nm) polycrystalline magnesium aluminate spinel were successfully performed in the 1100–1200 °C temperature range, under an applied stress of 120–200 MPa. It was found that the stress exponent and activation energy depended on temperature and applied stress, respectively. The deformed samples were characterized by high resolution scanning electron microscope (HRSEM) and high resolution transmission electron microscope (HRTEM). The results indicate that the creep mechanism was related to grain boundary sliding, accommodated by dislocation slip and climb. The experimental results, extrapolated to higher temperatures and lower stresses, were in good agreement with data reported in the literature.

Keywords: creep; spinel; SPS

1. Introduction

The use of spark plasma sintering (SPS) has continuously expanded over the past 20 years thanks to its excellent sintering capabilities. A special configuration of SPS tooling, described in our previous work [1,2], makes it possible to apply uniaxial pressure up to 1 GP during the sintering process. Sintering under high pressure allows for significant reduction of processing temperatures and fabrication of nano-structured ceramics. It was reported [1] that nano-structured magnesium aluminate spinel specimens, possessing a unique combination of optical and mechanical properties, could be fabricated under a uniaxial pressure of 400 MPa at 1200 °C. One of the main densification mechanisms acting in the final stage of sintering under elevated pressure is high temperature deformation (creep) of ceramic particles or grains [3]. The creep behavior of polycrystalline magnesium aluminate spinel and its capability to undergo superplastic deformation at relatively high temperatures (1300–1800 °C) over a wide range of applied stresses (1–200 MPa) have been investigated [4–11]. However, to the best of our knowledge, there is no data on creep behavior under conditions close to those that are applied during the high pressure SPS process. The data output of the SPS system includes temperature, applied pressure, relative punch displacement (RPD) and electric pulse parameters (*i.e.*, voltage, mode of current, frequency, *etc.*). In principle, the SPS apparatus is a high temperature dilatometer and can be used for the investigation of mechanical properties of ceramics at high temperatures. The accuracy of RPD measurements (about 1 μm) is suitable for high temperature experiments, such as creep. In the present study, an SPS apparatus was used to investigate the creep behavior of magnesium aluminate spinel for the first time.

2. Materials and Experimental Procedures

Magnesium aluminate spinel samples intended for creep testing were fabricated by SPS (HP-D10, FCT Systems, Rauensein, Germany) from a commercial $\text{MgO} \cdot \text{Al}_2\text{O}_3$ powder (S30CR Baikowski Chimie, La Blame de Silingy, France) with a specific surface area of $30 \text{ m}^2/\text{g}$, impurities levels of 10, 10, 20 and 5 ppm for Fe, Na, Si and Ca, respectively. SPS was performed inside a graphite die with 12 mm height and 20 mm diameter. The sintering parameters were a sintering temperature of $1300 \text{ }^\circ\text{C}$, a dwell time of 20 min, a heating rate of $10 \text{ }^\circ\text{C}/\text{min}$, an applied pressure of 60 MPa and a cooling rate of $50 \text{ }^\circ\text{C}/\text{min}$. The sintered samples were fully dense, with a grain size of about 250 nm. The spinel samples were precisely machined into a cylindrical geometry 12 mm in height and 6 mm in diameter. The creep experiments were conducted in the SPS apparatus with a DC pulse-mode current pattern (pulse 5 ms and pause 2 ms). A non-constrained sample was placed inside the high pressure SPS tooling, which consisted of an outer graphite die (outer diameter, 50 mm) and an inner die made of silicon carbide. The silicon carbide die had 10 mm inner and 20 mm outer diameters. A K-type thermocouple was inserted through the outer graphite die and placed in contact with the inner SiC die. Samples were heated to the initial temperature of $1100 \text{ }^\circ\text{C}$ at a heating rate of $200 \text{ }^\circ\text{C}/\text{min}$. Each compression creep experiment was conducted under constant pressures of 120, 150 and 200 MPa at various temperatures of 1100, 1150 and $1200 \text{ }^\circ\text{C}$, with a dwell time of about 2 h. The microstructure of the polished and thermally etched ($1400 \text{ }^\circ\text{C}$ for 10 min under ambient atmosphere) samples was examined using a high resolution scanning electron microscope (HRSEM; JSM-7400, JEOL, Tokyo, Japan) The grain size was estimated by Thixomet software (Thixomet, St.-Petersburg, Russia) for image analysis [12,13]. Samples for high resolution transmission electron microscope (HRTEM) analysis were prepared by a focused ion beam (FIB; Helios NanoLab 600, FEI, Hillsboro, OR, USA) and examined using a high resolution transmission electron microscope (HRTEM; JEM-2010F, JEOL, Tokyo, Japan).

3. Results and Discussion

3.1. Strain Rate

Creep curves for spinel were obtained from the experimental data recorded by the SPS system. RPD was converted to strain according to the initial specimen height (Figure 1).

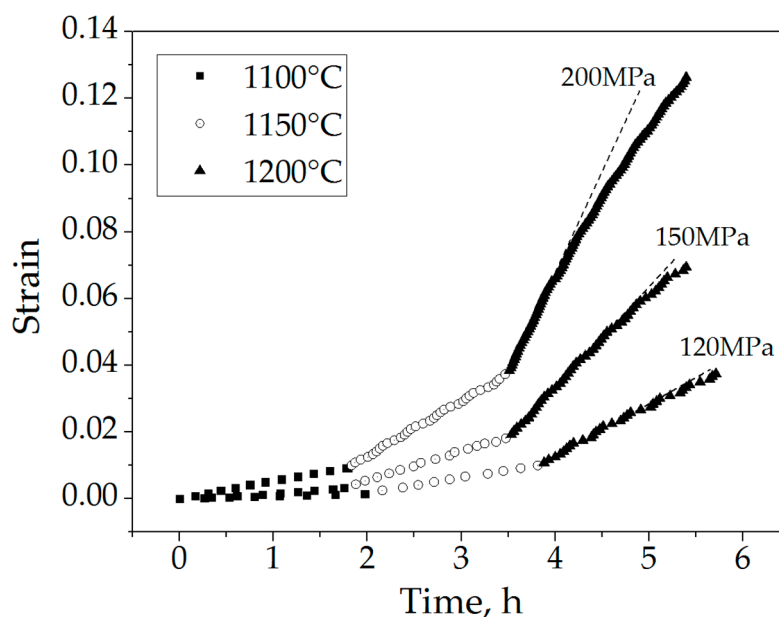


Figure 1. Creep curves for spinel under pressures of 120–200 MPa in the 1100–1200 °C temperature range. The dashed lines indicate change of the slope.

Each creep curve consists of three domains, each related to the creep at various temperatures, and which changed during the course of the experiment. At low temperatures (reflected as the first domain of the creep curves), the initial deformation was extremely low and almost undetectable. For the other curve domains, the material was already in the steady stage of creep. The softening of the material was clearly observed as an increased slope of the curves with temperature. Finally, the hardening effect can be observed at high temperature and upon high strain (reflected in the continuous change/decrease of the slopes and indicated by the dashed line in Figure 1). Strain rates were determined from the slopes of the quasi-linear steady-state portions [4,8,11] of each domain and are presented as a function of temperature in Figure 2.

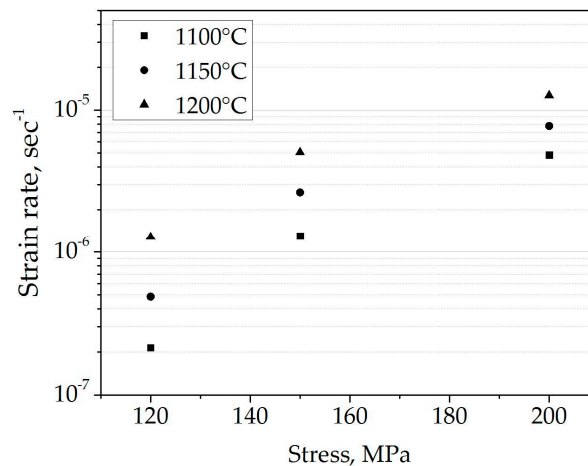


Figure 2. Creep rates of spinel as a function of pressure, tested at various temperatures.

The creep rates obtained at the tested temperatures and stress range fit the deformation-mechanism map for magnesium aluminate spinel [14] and correspond to the region of power law creep [15]. Therefore, the data were analyzed according to the general creep equation:

$$\dot{\epsilon} = A\sigma^n \exp\left(\frac{-Q}{RT}\right) \quad (1)$$

where $\dot{\epsilon}$ is the creep rate, A is the creep constant, σ is the applied load, n is the stress exponent, Q is the activation energy, R is the gas constant and T is the temperature. The creep parameters (*i.e.*, Q and n) can vary with experimental conditions (*i.e.*, applied stress and temperature), along with other factors, such as composition and microstructure of the tested materials [16]. The experimental data for different temperatures and stresses allow for estimations of stress exponent and apparent activation energy values according to:

$$\ln(\dot{\epsilon}) = \ln A + n \ln(\sigma) - \frac{Q}{RT} \quad (2)$$

3.2. Stress Exponent

The values of the stress exponent (Table 1) were determined from the slopes of the curves presented in Figure 3.

Table 1. Values of the stress exponent at various temperatures.

Temperature (°C)	Stress Exponent (n)
1100	3.48 ± 0.1
1150	2.64 ± 0.26
1200	1.87 ± 0.15

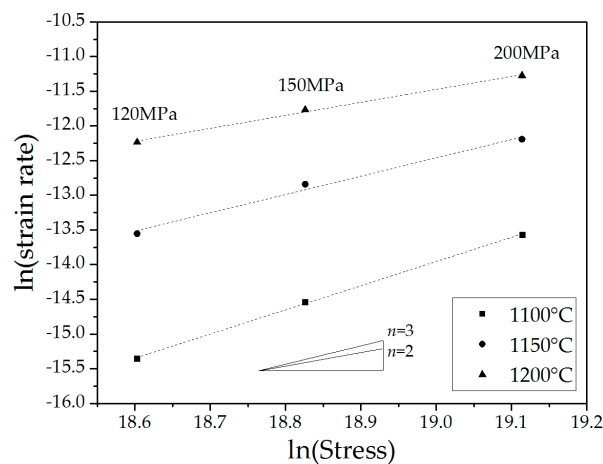


Figure 3. $\ln(\text{strain rate})$ vs. $\ln(\text{stress})$ for spinel tested under 120, 150 and 200 MPa.

The stress exponent values obtained are in good agreement with those previously reported [4–11]. Temperature-dependence of the stress exponent was also observed [9] and was attributed to changes in the creep mechanism. For low stress exponent values ($n \approx 1$), creep is governed by the diffusional flow of ions [17]. For higher stress exponent values ($n \approx 2$), creep of the fine polycrystalline ceramics is mostly controlled by grain boundary sliding (GBS) [18], as was clearly demonstrated for polycrystalline alumina [19,20]. GBS, however, has to be accommodated by an additional process [21,22], such as intergranular slip and the subsequent climb of dislocations [23]. According to the apparent values of the stress exponent, GBS was the dominant mechanism in the 1150–1200 °C temperature range. The higher stress exponent ($n \approx 3.5$) obtained at the lowest temperature considered (1100 °C), could be attributed to formation of triple-point folds [24,25]. Another possibility is the reduced contribution of GBS [26], with a larger percentage of deformation being carried out by dislocation slip and climb ($4 > n > 3$) [15].

3.3. Activation Energy

The temperature-dependence of the creep rate under various stresses allowed for estimation of the apparent activation energy of the process (Figure 4).

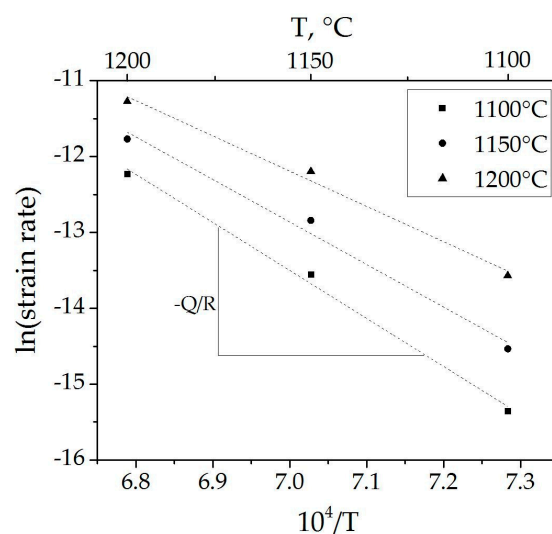


Figure 4. Strain rate vs. the reciprocal of temperature.

Calculated apparent activation energy values are presented in Table 2.

Table 2. Apparent activation energies for polycrystalline magnesium aluminate spinel.

Applied Stress (Mpa)	Activation Energy (Q) (kJ/mol)
120	526 ± 35
150	465 ± 50
200	387 ± 36

The apparent activation energy values for creep in spinel under our experimental conditions, as well as their dependence on the stress applied (Figure 5), are in good agreement with previously reported data [4,5,7]. The decrease in activation energy with applied stress may be attributed to competition between the GBS and dislocation creep mechanisms of deformation. Under higher applied stress, more dislocations are generated within the material, a process which requires relatively lower thermal activation, making the effect of temperature less pronounced. At lower applied stress, the amount of dislocations decreases, while the role of ion diffusion increases. As such, the effect of temperature becomes more significant.

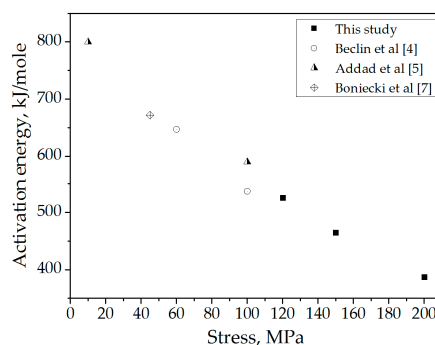


Figure 5. Apparent activation energy as a function of stress.

The average creep constant $A (=8.43 \times 10^{-11} \pm 1.38 \times 10^{-11} \text{ sec}^{-1} \cdot \text{MPa}^{-n})$, which depends on the material and only slightly on pressure and temperature was estimated based on the stress exponent and activation energy values obtained. The experimental results were extrapolated for a wider range of strain rates (*i.e.*, for lower stresses and higher temperatures), to fit with experimental data reported in the literature [4–6]. The extrapolated data, along with our experimental results and the data reported in literature, are presented in Figure 6.

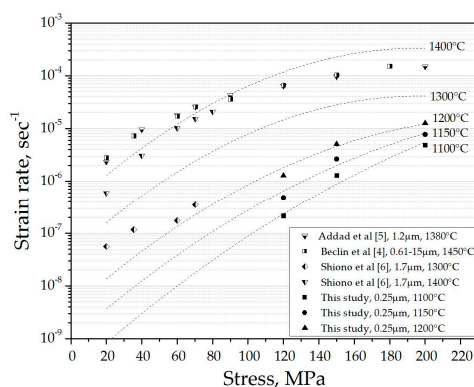


Figure 6. Strain rate *vs.* applied stress. Extrapolation of our experimental data (dashed lines) and values reported in the literature for various creep conditions and grain sizes (indicated in the legend) are shown.

The extrapolated values of the strain rate are in a good agreement with previously reported data. Some scattering of the experimental results may be attributed to differences in creep conditions, particularly the grain sizes of the tested samples.

It should be noted that creep was tested in the SPS apparatus under a small electric field ($\sim 70 \text{ V} \cdot \text{cm}^{-1}$). The good agreement noted between our results and those reported obtained using a conventional testing procedure indicates that the electric field contributes only a negligible or no effect on the creep of the fine grain polycrystalline spinel.

HRSEM images of polished and thermally etched samples before and after creep deformation are presented in Figure 7.

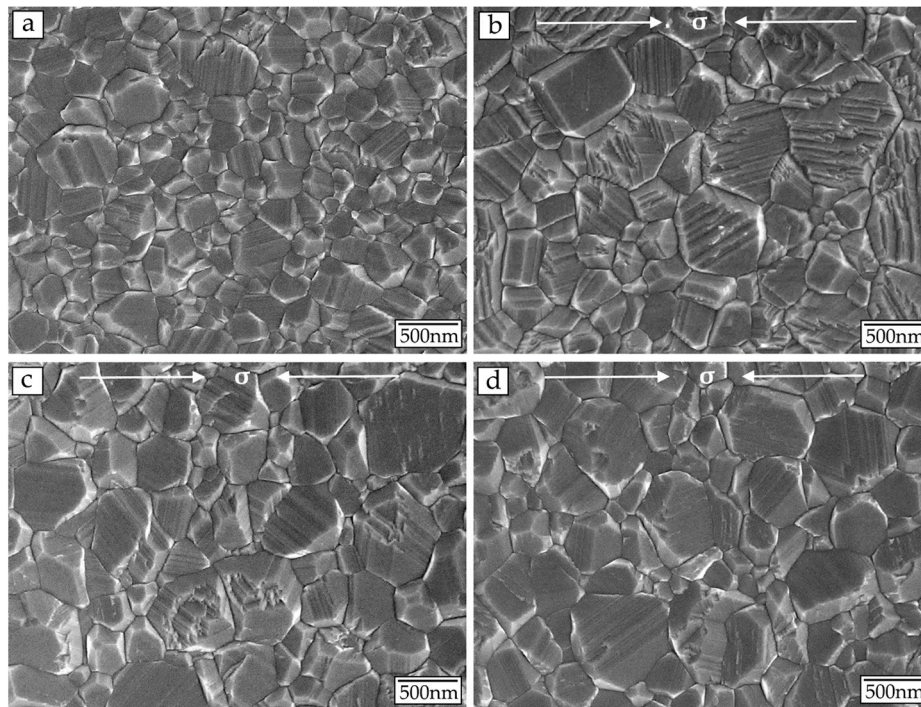


Figure 7. High resolution scanning electron microscope (HRSEM) images of the spinel samples: before creep (a); after creep at 1100–1200 °C (4% strain) under 120 (b); (7% strain) 150 (c) and (13% strain) 200 MPa (d). Compression direction is marked.

The initial microstructure (Figure 7a) consisted of fine equiaxed grains with an average size of about 250 nm. After the creep test, the average grain size was larger (400 nm) and grain shape remained equiaxed with no directional growth (Figure 7b–d). According to [27], this implies that GBS was the main mechanism by which the samples were deformed during creep under our testing conditions. We assume that in this range of grain size its effect on creep rate was not significant.

The appearance of faceting morphology of spinel grains is attributed to the preferential thermal etching of {111} planes, which have higher surface energy than either the {100} or {110} planes. The faceting morphology was detected in both before and after creep samples and does not depend on the grain deformation [28].

To clarify the creep mechanism, HRTEM analysis of deformed samples after creep under pressures of 120 and 200 MPa, was performed (Figure 8).

Several types of distinctive features of creep were found in all examined samples. The formation of triple point voids and displaced triple points (Figure 8a,b) provided strong evidence for GBS [29]. Moreover, grain separation, appeared as grain boundary cavities, was also observed, which is typical for creep with no glassy phase at the grain boundaries [25]. These observations confirmed that substantial GBS had taken place during creep under our testing conditions. Dislocations and

dislocation pile-ups were also observed, especially in that sample subjected to 200 MPa pressure (Figure 8c). By using the weak-beam dark field (WBDF) method that allows pronounced contrast for dislocations [30], high dislocation densities were found within the grains at $g = 440$ (Figure 8d), which is known to be the preferred dislocation slip plane in spinel [11,30,31]. This may indicate that a dislocation mechanism was involved at the relatively higher stress level.

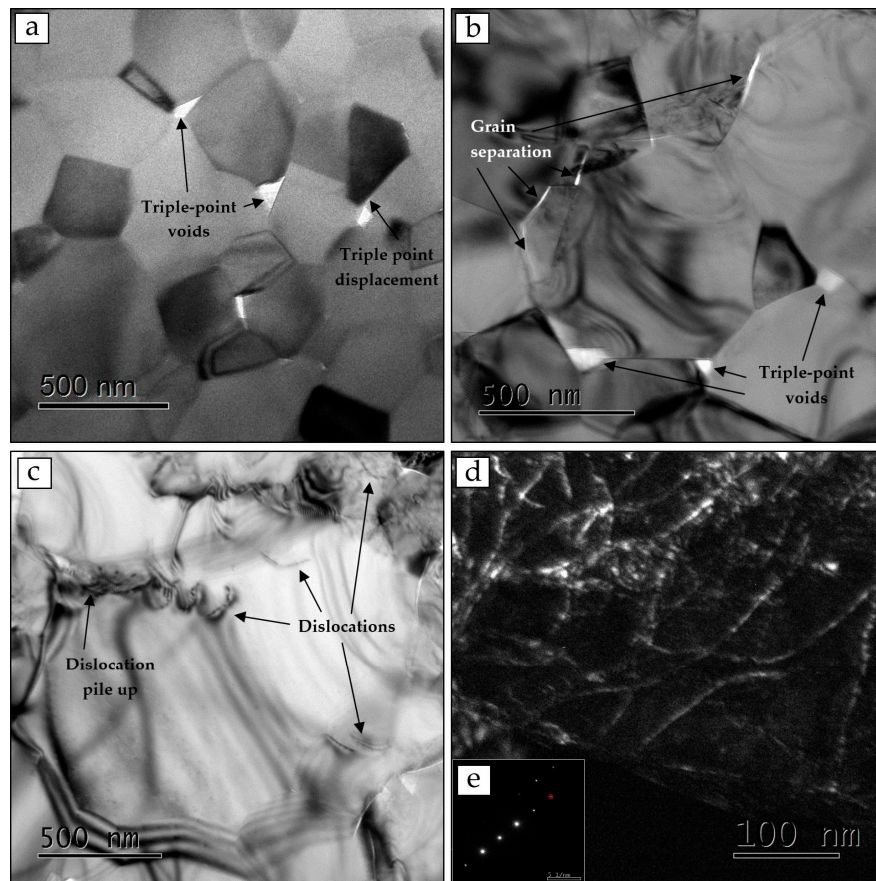


Figure 8. High resolution transmission electron microscope (HRTEM) images of spinel samples after deformation at 1100–1200 °C. Under 120 MPa (4% strain) triple-point voids and displaced triple points are shown (a); under 200 MPa (13% strain) grain separation and sliding along the grain boundaries (b) and dislocations (c) are shown. A weak-beam dark field (WBDF) image for $g = 440$ shows the high dislocation density within the grain after creep in response to 200 MPa pressure (d); The selected area diffraction pattern is presented in the insert (e). The examined cross-sections were perpendicular to the compression axis.

4. Conclusions

Compression creep testing of polycrystalline magnesium aluminate spinel was successfully performed for the first time using an SPS apparatus. The stress exponent value decreased from 3.5 to 2 with temperature in the 1100–1200 °C range. Likewise, the apparent activation energy value decreased from 526 to 387 kJ/mol with applied stress in the 120–200 MPa range. Our results and the data predicted by extrapolation are in a good agreement with values reported in the literature. The microstructure of the deformed samples, consisting of an equiaxed grain structure, indicated that GBS operated during creep. HRTEM examination confirmed that the deformation occurred by GBS accommodated by dislocation movement.

Author Contributions: Barak Ratzker was responsible for literature review, prepared samples for characterization, analyzed microstructural images, and processed the experimental data. Maxim Sokol designed the experiments, prepared samples for creep testing, analyzed the creep data and interpreted the results. Sergey Kalabukhov fabricated samples by SPS and conducted creep experiments. Nachum Frage supervised the work and interpreted the results. All authors contributed to the writing of the paper.

Conflicts of Interest: The authors declare no conflict of interest.

References

1. Sokol, M.; Kalabukhov, S.; Dariel, M.P.; Frage, N. High-pressure spark plasma sintering (SPS) of transparent polycrystalline magnesium aluminate spinel (PMAS). *J. Eur. Ceram. Soc.* **2014**, *34*, 4305–4310. [[CrossRef](#)]
2. Sokol, M.; Kalabukhov, S.; Kasiyan, V.; Dariel, M.P.; Frage, N. Functional properties of Nd:YAG polycrystalline ceramics processed by High-Pressure Spark Plasma Sintering (HPSPS). *J. Am. Ceram. Soc.* **2016**, *99*, 802–807. [[CrossRef](#)]
3. Wilkinson, D.S.; Ashby, M.F. Pressure sintering by power law creep. *Acta Metall.* **1975**, *23*, 1277–1285. [[CrossRef](#)]
4. Beclin, F.; Duclos, R.; Crampon, J.; Valin, F. Microstructural superplastic deformation in MgO·Al₂O₃ spinel. *Acta Metall. Mater.* **1995**, *43*, 2753–2760. [[CrossRef](#)]
5. Addad, A.; Beclin, F.; Crampon, J.; Duclos, R. High temperature deformation of spinel-zirconia composites effect of zirconia content. *Ceram. Int.* **2007**, *33*, 1057–1063. [[CrossRef](#)]
6. Shiono, T.; Ishitomi, H.; Okamoto, Y.; Nishida, T. Deformation mechanism of fine-grained magnesium aluminate spinel prepared using and alkoxide precursor. *J. Am. Ceram. Soc.* **2000**, *83*, 645–647. [[CrossRef](#)]
7. Boniecki, M.; Librant, Z.; Wajler, A.; Wesolowski, W.; Weglarz, H. Fracture toughness, strength and creep of transparent ceramics at high temperature. *Ceram. Int.* **2012**, *38*, 4517–4524. [[CrossRef](#)]
8. Beclin, F.; Duclos, R.; Crampon, J.; Valin, F. Superplasticity of HIP MgO·Al₂O₃ spinel: Prospects for superplastic forming. *J. Eur. Ceram. Soc.* **1997**, *17*, 439–445. [[CrossRef](#)]
9. Choi, M.D.; Palmou, H., III. *Flow and Fracture of Hot-Pressed Polycrystalline Spinel at Elevated Temperatures*; No. TR-2; Dept. of Engineering Research, North Carolina State University: Raleigh, NC, USA, 1965.
10. Panda, P.C.; Raj, R.; Morgan, P.E.D. Superplastic deformation in fine-grained MgO·Al₂O₃ spinel. *J. Am. Ceram. Soc.* **1985**, *68*, 522–529. [[CrossRef](#)]
11. Morita, K.; Hiraga, K.; Kim, B.; Suzuki, T.S.; Sakka, Y. Strain softening and hardening during superplastic-like flow in a fine-grained MgAl₂O₄ spinel polycrystal. *J. Am. Ceram. Soc.* **2004**, *87*, 1102–1109. [[CrossRef](#)]
12. Kazakov, A.; Luong, N.; Kazakova, E.; Zorina, E. Thixomet image analyzer for characterization of 2D and 3D materials structure. *Microstruct. Sci.* **2000**, *27*, 133–142.
13. Kazakov, A.; Luong, N. Characterization of semisolid materials structure. *Mater. Charact.* **2001**, *46*, 155–161. [[CrossRef](#)]
14. Frost, H.J.; Ashby, M.F. *Deformation-Mechanism Maps: The Plasticity and Creep of Metals and Ceramics*; Pergamon Press: Oxford, UK, 1982; pp. 105–110.
15. Weertman, J. Theory of steady-state creep based on dislocation climb. *J. Appl. Phys.* **1955**, *26*, 1213–1217. [[CrossRef](#)]
16. Barsoum, M.W. *Fundamentals of Ceramics*; IOP Publishing Ltd.: Bristol, UK, 2003; pp. 400–432.
17. Chokshi, A.H. Diffusion creep in oxide ceramics. *J. Eur. Ceram. Soc.* **2002**, *22*, 2469–2478. [[CrossRef](#)]
18. Langdon, T.G.R. The role of grain boundaries in high temperature deformation. *J. Mater. Sci. Eng.* **1993**, *166*, 67–79. [[CrossRef](#)]
19. Cannon, W.R.; Sherby, O.D. Creep behavior and grain boundary sliding in polycrystalline Al₂O₃. *J. Am. Ceram. Soc.* **1977**, *60*, 44–47. [[CrossRef](#)]
20. Ruano, O.A.; Wadsworth, J.; Sherby, O.D. Deformation of fine-grained alumina by grain boundary sliding accommodated by slip. *Acta Mater.* **2003**, *51*, 3617–3634. [[CrossRef](#)]
21. Langdon, T.G. Grain boundary sliding as a deformation mechanism during creep. *Philos. Mag.* **1970**, *22*, 689–700. [[CrossRef](#)]
22. Raj, R.; Ashby, M.F. On grain boundary sliding and diffusional creep. *Metall. Trans.* **1971**, *2*, 1113–1127. [[CrossRef](#)]
23. Ball, A.; Hutchison, M.M. Superplasticity in the aluminium-zinc eutectoid. *Met. Sci.* **1969**, *3*, 1–7. [[CrossRef](#)]

24. Gifkins, R.C. Grain boundary sliding and its accommodation during creep and superplasticity. *Metall. Trans.* **1976**, *7*, 1225–1232. [[CrossRef](#)]
25. Cannon, W.R.; Langdon, T.G. Review creep of ceramics part 1 mechanical characteristics. *J. Mater. Sci.* **1983**, *18*, 1–50.
26. Cannon, W.R.; Langdon, T.G. Review creep of ceramics part 2 an examination of flow mechanisms. *J. Mater. Sci.* **1988**, *23*, 1–20. [[CrossRef](#)]
27. Langdon, T.G. Grain-boundary sliding in ceramics. *J. Am. Ceram. Soc.* **1972**, *55*, 430–431. [[CrossRef](#)]
28. Browne, D.; Li, H.; Giorgi, E.; Dutta, S.; Biser, J.; Vinci, R.P.; Chan, H.M. Templated epitaxial coatings on magnesium aluminate spinel using sol gel method. *J. Mater. Sci.* **2009**, *44*, 1180–1186. [[CrossRef](#)]
29. Heuer, A.H.; Cannon, R.M.; Tighe, N.J. Plastic deformation in fine-grain ceramics. In Proceedings of the 15th Sagamore Army Materials Research Conference, Ultrafine-Grain Ceramics, Raquette Lake, NY, USA, 20–23 August 1968; Burke, J.J., Reed, N.L., Weiss, V., Eds.; Syracuse University Press: New York, NY, USA, 1970; pp. 339–365.
30. Ting, C.J.; Lu, H.Y. Hot-pressing of magnesium aluminate spinel—II. Microstructure development. *Acta Mater.* **1999**, *47*, 831–840. [[CrossRef](#)]
31. Mitchell, T.E. Dislocations and mechanical properties of MgO-Al₂O₃ spinel single crystals. *J. Am. Ceram. Soc.* **1999**, *82*, 3305–3316. [[CrossRef](#)]



© 2016 by the authors; licensee MDPI, Basel, Switzerland. This article is an open access article distributed under the terms and conditions of the Creative Commons Attribution (CC-BY) license (<http://creativecommons.org/licenses/by/4.0/>).